High-pressure effects in the layered semiconductor germanium selenide

H.C. Hsueh, H.Vass, S.J. Clark, G.J. Ackland, and J. Crain
Department of Physics and Astronomy The University of Edinburgh, Mayfield Road, Edinburgh, Scotland EH9 3JZ, United Kingdom
(Received 11 November 1994; revised manuscript received 28 February 1995)

We report the results of *ab initio* total-energy pseudopotential calculations, high-pressure angle-dispersive powder x-ray diffraction, and vibrational spectroscopy measurements on the IV-VI layered semiconductor germanium selenide (GeSe). The calculated hydrostatic pressure dependence of the crystal structure is found to be in good agreement with the results of high-resolution x-ray structural studies. In contrast to previous reports, no evidence of a pressure-induced first-order structural phase transition is found up to 130 kbar. However, a metallization transition is predicted in our electronic structure calculations. This is consistent with reports of a large resistivity drop at high pressure. The rigid-layer vibrational shear mode is also investigated by *ab initio* methods within the rigid-layer mode approximation and the freqency is found to be in fair agreement with our Raman scattering results at ambient pressure. At higher pressures the calculated frequency is substantially overestimated in the calculations.

I. INTRODUCTION

The nine binary IV-VI materials (Ge,Sn,Pb)-(S,Se,Te) adopt one of three related crystal structures at ambient pressure. The heaviest class of these materials (the Pb chalcogenides) adopts the rocksalt structure under normal conditions. At high temperature, SnTe and GeTe also exist in the rocksalt structure but at low temperature, these compounds possess a rhombohedral structure similar to that found in the isoelectronic elemental semimetals As, Sb, and Bi. The four lighter compounds (Ge,Sn)-(S,Se) adopt an orthorhombic structure, which is closely related to that of black phosphorous.

There has been a considerable amount of theoretical effort devoted to understanding the origin of the observed phase boundaries in the IV-VI materials. For example, it appears that the stability of the rocksalt structure of the Pb chalcogenides is due to relativistic effects that enhance the *s-p* energy splitting. This effect suppresses the hybridization of these levels[1] and precludes the formation of directional *s-p* orbitals. These relativistic effects become less important for the lighter materials and as a result, the *s-p* splitting is reduced, allowing for the possibility of covalent bonds.

Layered covalent structures are known to characterize (Ge,Sn)-(S,Se) at ambient pressure. Littlewood has shown that the structural trends in the binary IV-VI compounds at ambient pressure can be accounted for through consideration of the ionicity and covalency of the materials.[1] This led to the successful structural classification of the binary IV-VI materials, using two coordinates derived from orbital radii.

Experimental structural studies at high pressure, using energy-dispersive x-ray diffraction, have been performed on several members of the IV-VI family.[2] It was found that PbS, PbSe, and PbTe undergo structural phase transitions from rocksalt to an orthorhombic structure at pressures of 22, 45, and 60 kbar, respectively. The high pressure structures of PbS and PbSe are of the thallous iodide type, while the high-pressure structure of PbTe appear to be similar to that of GeS.[3] A further structural transition in PbTe to a CsCl-type phase has also been observed at pressures above 160 kbar.[4] The layered orthorhombic IV-VI compounds were not observed to undergo any structural transitions up to 340 kbar which is the highest pressure at which these materials have been studied.

High-pressure electrical measurements by Bhatia *et al.*[5] on single-crystal GeSe revealed a drop in resistivity of five orders of magnitude at 60 kbar from which these authors concluded that a first-order transition had occurred. Upon downloading to ambient pressure, x-ray diffraction patterns indicated that the recovered samples possessed an NaCl-like structure (a = 7.37 Å). Transport measurements revealed that the pressure-induced metallic character was retained down to ambient pressure. These results, therefore, appear to be at variance with those of Ref. 2 based on energy-dispersive diffraction.

It is also well established that the vibrational spectra of layered or "quasi-two-dimensional" crystals are characterized by low-frequency optical phonons. These modes are attributed to vibrations in which the layers move as approximately rigid units relative to each other. They can be routinely studied using Raman scattering.[6,7,9,10] There are two shear modes in which adjacent rigid layers move parallel to each other in the a and b directions and one compressive vibration in which the layers vibrate against each other parallel to the c axis.

The pressure effect on rigid-layer vibrational modes is particularly dramatic as compression preferentially enhances the weak interlayer bonding. There have been few high-pressure studies of the vibrational properties of such modes in the IV-VI semiconductor family; however, the pressure dependence of the Raman active modes in GeS and GeSe has been measured.[7] The maximum pres-

sure attained in this study was 7 kbar, therefore, no conclusions could be drawn regarding pressure-induced structural transitions. Nevertheless, it was shown that the pressure coefficients of the rigid-layer modes were an order of magnitude larger than those of the intralayer modes.

There has, however, been relatively little theoretical attention focused on the high-pressure effects in the IV-VI compounds. As discussed previously, these effects are expected to be particularly important in layered materials. To our knowledge, there have been no *ab initio* calculations of high-pressure effects in this family.

The importance of understanding pressure-induced structural, electronic, and vibrational effects in layered semiconductors, in general, and the conflicting accounts of the pressure effect in GeSe, in particular, provides the motivation for the present work. In this paper, we apply *ab initio* total-energy pseudopotential methods, high-pressure angle-dispersive powder diffraction, and vibrational spectroscopy in order to study pressure-induced phenomena in GeSe.

The paper is organized in the following order. Structural details of GeSe are given in the next section. The details of our computational method are then outlined and a discussion of the experimental methods is given. We next describe the results of our total energy calculations on structural stability and compare them to experimental results. High pressure vibrational spectroscopic results are then presented and compared to the results of our calculations.

II. STRUCTURAL DETAILS

At ambient pressure GeSe adopts a layered orthorhombic crystal structure (space group $Pcmn$, D_{2h}^{16}).[8] There are eight atoms contained in the unit cell. The unit cell parameters are $a = 4.38$ Å, $b = 3.82$ Å, and $c = 10.79$ Å. An illustration of the GeSe crystal structure is shown in Figs. 1(a) and (b). The structure is completely defined by the additional specification of two free atomic positional parameters (u and v) for each species. Ge and Se atoms are located at positions $(u_{\mathrm{Ge}}, \frac{1}{4}, v_{\mathrm{Ge}})$ and $(u_{\mathrm{Se}}, \frac{1}{4}, v_{\mathrm{Se}})$, respectively. The crystal structure is often considered as being a distortion of the rocksalt configuration. This distortion leads to approximately threefold coordination of atoms of unlike species in a given double layer. The ambient pressure bond lengths are 2.582 Å and 2.538 Å.

There are three bond angles in this structure. One lies almost in the a-b plane and has a value of 95.4°. There are two other intralayer bond angles with verticies at either the Ge or Se atoms. These bond angles are 90.8° and 103.6°, respectively.

In the same double layer, there are two more next-nearest neighbors of unlike species at a distance of approximately 3.3 Å away. More distant neighbors are located in the adjacent double layer. Two of these neighbors are of the same species and the other is of a different species.

The layers of covalently bonded Ge-Se pairs interact weakly and GeSe samples are easily cleaved in planes perpendicular to the c axis. This layered character is the source of the substantial anisotropy in the optical properties of GeSe, which has been the focus of several experimental investigations.[11–13] Two other length scales will be relevant in our later discussion of the structural

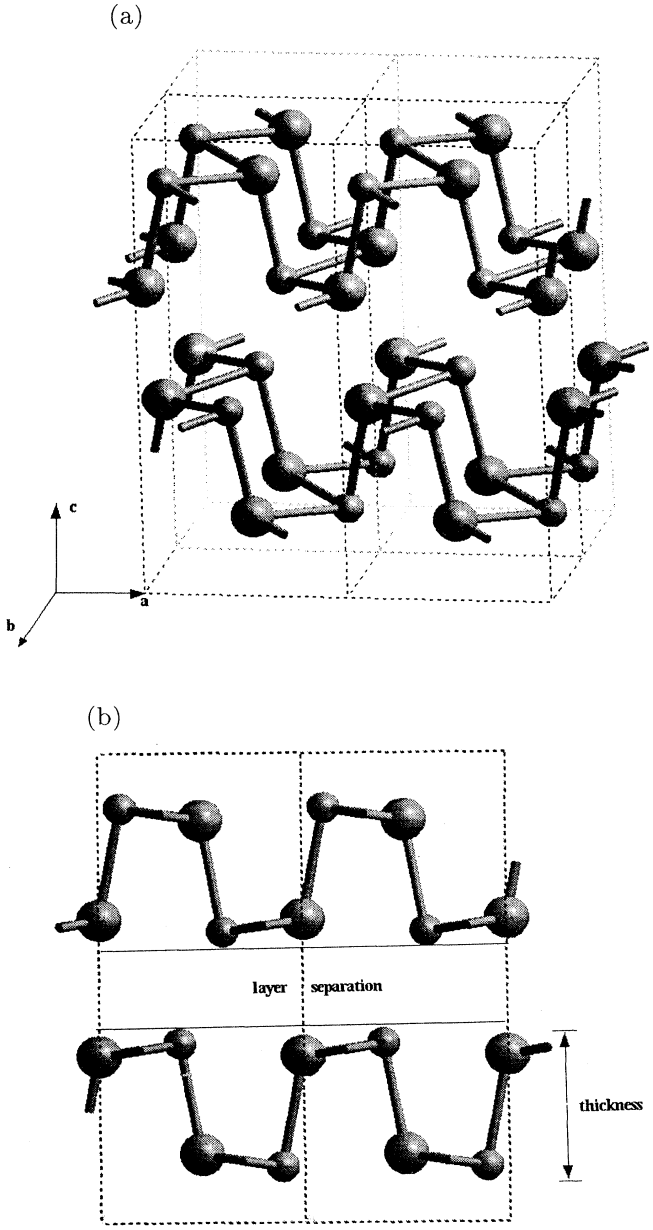

FIG. 1. (a) Illustration of the GeSe orthorhombic crystal structure (space group $Pcmn$). Four unit cells are shown (doubled in the a and b direction). The layered character and atom coordination are evident. The unit cell parameters have been determined by single-crystal methods (Ref. 8) to be a= 4.38 Å, b=3.82 Å, and c=10.79 Å. The structure is completely specified by four internal atomic positional parameters, such that the atoms are located at positions $(u_{\mathrm{Ge}}, \frac{1}{4}, v_{\mathrm{Ge}})$ and $(u_{\mathrm{Se}}, \frac{1}{4}, v_{\mathrm{Se}})$. In (b) is shown a projection of the structure along the b axis, showing the intralayer thickness and interlayer separation.

properties of GeSe under pressure. These are the interlayer separation and intralayer thickness. These are independent of the a and b cell parameters and are given by $2(1 - v_{Ge})c$ and $2(v_{Ge} - \frac{3}{4})c$, respectively.

III. COMPUTATIONAL METHODS

To perform our calculations, we have employed the *ab initio* total-energy pseudopotential method. We use the local density approximation (LDA) to describe the electronic exchange-correlation interactions based on the parametrization of Perdew and Zunger.[14] The valence electron wave functions are expanded in a plane wave basis set up to a cutoff energy of 300 eV. This corresponds to approximately 2500 plane waves per band per k point. The nonlocal ionic pseudopotentials are in the Klienman-Bylander form[15] and were generated by the Kerker method.[16] A preconditioned conjugate gradients method was used to minimize the total energy of the system.

At all volumes, the ionic positions were relaxed under the influence of the Hellmann-Feynman forces until no force component exceeded 0.01 eV/Å. The conjugate gradient method was also used for this ionic relaxation. This gave a total-energy convergence to better than 0.01 eV/atom. We have repeated this calculation using many different lattice parameters in order to find the full hydrostatic pressure response.

The Brillouin zone (BZ) integrations are performed using the special points scheme of Monkhorst and Pack,[17] where we symmetrize the charge density every iteration to reflect the $D_{2h}^{16}(Pcmn)$ group symmetry of the layered GeSe structure. This symmetry constraint is implemented by averaging the charge density from each equivalent point in the BZ, as defined by the point group operations of the structure, in order to construct a charge density in the irreducible wedge, which is then used to generate a charge density having the correct symmetries for the structure. This ensures that the Hellmann-Feynman forces are also constrained to this symmetry.

It is found that the problem of k-point sampling used to perform the integrations over the BZ is particularly acute in this case. We have performed several calculations with different k-point sets to ensure the convergence of our results. Our k-point convergence tests are summarized in Table I. The structural parameters have been determined by fitting the energy vs volume curve to the Murnaghan equation of state. Note that, although the sets containing 8 and 20 points converge to give the same total energy, the relaxed volumes differ by several tenths of Å^3. This indicates that ensuring the convergence of total energies with respect to k-point set is not a stringent enough requirement. Further evidence for this is illustrated in Fig. 2, where the total energy vs volume curves are shown. It can be seen that the bulk modulus (second derivative of the curve) is also softer in the eight point set than in the 20 point set. We have found our calculations to be completely converged using the $4 \times 4 \times 10$ set of k points and it is this set that we use in the following calculations. A thorough description of the computational methods employed in these calculations can be found in the recent review by Payne *et al.*[18] We next discuss the details of the main experimental methods used in this study.

TABLE I. Minimum total energies per atom (E_0) and their corresponding volumes per atom (V_0) for various Monkhorst-Pack k-point sets. The second column shows the number of k points in the irreducible zone of the GeSe structure that each set gives.

k-pt set	Pts in irred. zone	E_0	V_0
$2 \times 4 \times 4$	4	-183.56	20.63
$4 \times 4 \times 4$	8	-183.46	21.49
$4 \times 4 \times 10$	20	-183.46	20.71

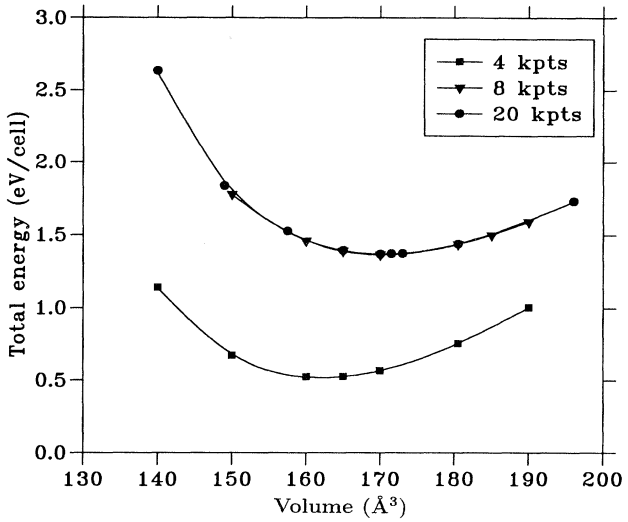

FIG. 2. Graphs showing relative total energy vs atomic volume for several different special k-point sets. The results for the 4-, 8-, and 20-k-point set are shown as squares, triangles, and circles, respectively. Note that, for the 8-k-point set, the total energy has already converged, but 20-k-points are necessary to determine the optimum unit cell volume. Results of these convergence tests are summarized in Table I. The unit cell parameters were not optimized at every volume in these convergence tests. Therefore, the curves do *not* represent the hydrostatic pressure response of the GeSe structure.

IV. EXPERIMENTAL METHODS

A. High-pressure angle-dispersive powder x-ray diffraction

The pressure dependence of the GeSe crystal structure was studied experimentally using synchrotron powder x-ray diffraction and image plate area detectors for optimal signal to noise ratios and accurate relative peak intensities. The latter is particularly important in situations where atomic positional parameters are to be determined

as a function of pressure. The powder sample was obtained by grinding a melt-grown single-crystal sample at liquid nitrogen temperature. The resulting powder was then loaded into a diamond anvil pressure cell along with a 4:1 methanol:ethanol mixture and a small chip of ruby which was used to determine pressure. The wavelength of the beam was set to 0.4652 Å using a Si(111) monochromator and the incident beam was collimated to a diameter of 75 μm. Determination of the cell dimensions and atomic positional parameters was made by least-squares fitting to the powder diffraction profile using the MPROF Reitveld refinement package.[19] Full details of the experimental apparatus, beamline optics, and data processing methods are given elsewhere.[20,21] The average exposure time used in these experiments was approximately 30 min.

B. High-pressure vibrational spectroscopy

Vibrational properties of GeSe were investigated using Raman spectroscopy up to a maximum pressure of 50 kbar. The 6764 Å line of a Kr^+ laser was used. For this study, measurements were made only on planes normal to the c axis. For this geometry, the rigid-layer A_g shear mode is accessible. Freshly cleaved surfaces were used and additional polishing was not required. Measurements normal to the a and b faces were not made in this study. Spectra were collected using a scanning Coderg T800 triple grating spectrometer in backscattering geometry. A standard diamond anvil pressure cell was used and the sample was loaded with a 4:1 methanol-ethanol mixture. Pressure determination was made by the ruby fluorescence method. In order to optimize the signal from the sample contained in the pressure cell, the beam was tightly focused onto the sample surface, using a small lens between the mirror and sample. The laser power was estimated to be between 50 and 60 mW at the sample. The sample chamber was flushed with argon gas to eliminate contamination from air signals. Prism filters were used to eliminate emission lines. The count time was 30 seconds per data point and the instrumental resolution was 1.5 cm^{-1}.

V. STRUCTURAL PROPERTIES

A. Ambient pressure structure of GeSe

The calculated total energy as a function of volume is shown in Fig. 3. At every unit cell volume the atomic positional parameters were relaxed under Hellmann-Feynman forces and the unit cell parameters were also optimized to minimize enthalpy. Thus, the curve represents the *hydrostatic* pressure response of GeSe.

The calculated equilibrium unit cell parameters were found to be a=4.293 Å, b = 3.744 Å, and c= 10.576 Å. Our experimentally determined lattice constants were found to be a = 4.385(5) Å, b = 3.836(4) Å, and c = 10.841(6) Å. Thus the calculated cell parameters are roughly 2% smaller than the corresponding room temperature values. Our calculations correspond to zero temperature values and at present, we are unaware of any measurement of the GeSe cell dimensions at low temperatures. However, we have measured the temperature dependence of the c-axis lattice parameter, using single-crystal methods, and find that it decreases to 10.790 Å, at a temperature of 135 K. Therefore, temperature effects can account for some of the discrepancy, but we believe that the dominant cause of the underestimate lies in the well known tendency of LDA methods to "overbind."

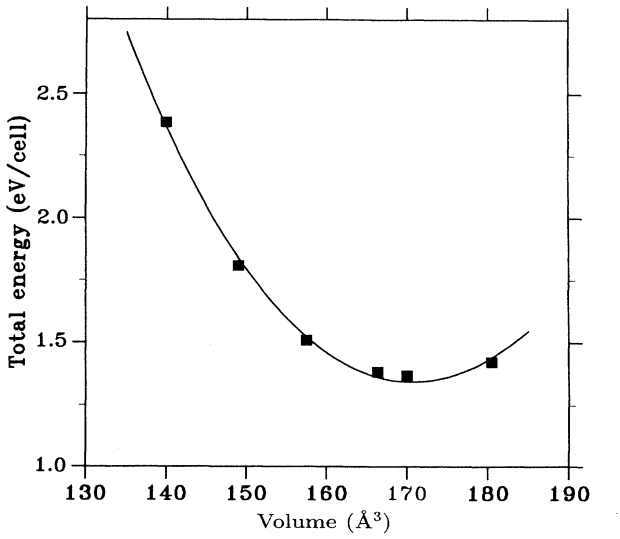

FIG. 3. Relative total energy vs unit cell volume as determined by *ab initio* calculations. At every volume, the four internal atomic positional parameters were relaxed under the influence of Hellmann-Feynman forces and the unit cell dimensions were also optimized to give the *hydrostatic* pressure response of GeSe. The solid line was determined by fitting the total energy vs unit cell volume curve to a Murnaghan equation of state (solid line).

We next consider the internal structural parameters at ambient pressure. The relaxed internal GeSe structure as predicted by our pseudopotential calculations corresponded to positional parameters given by u_{Ge} = 0.107, v_{Ge} = 0.882, u_{Se} = 0.494, and v_{Se} = 0.145. These values and the above-given cell parameters corrrespond to Ge-Se bond lengths of 2.542 Å and 2.547 Å. The calculated equilibrium bond angles are 90.4° for the bond in the a-b plane and 94.9° for the other intralayer bond. These bond angles and bond lengths compare well with those reported in Ref. 8, although our calculations suggest a slightly smaller difference between the two bond lengths at equilibrium. A detailed low-temperature structural study would be helpful in understanding the temperature effect on the Ge-Se bond distance.

As stated previously, in order to determine the atomic positional parameters from powder diffraction, it is necessary to record accurate relative intensities of the diffraction peaks. It should be noted that the layered character of the GeSe crystals may give rise to preferred orientation of the crystallites in the pressure cell. This is because the

TABLE II. Calculated structural parameters for the ambient pressure structure of GeSe. For comparison, the experimental results are also shown. The cell parameters (a, b, and c) are given in Angstroms and the positional parameters u_{Ge}, v_{Ge}, u_{Se}, and v_{Se} are given in fractional coordinates.

Method	a	b	c	u_{Ge}	v_{Ge}	u_{Se}	v_{Se}
Calculated	4.293	3.744	10.576	0.107	0.882	0.498	0.145
Expt.[a]	4.38	3.82	10.79	0.106	0.879	0.503	0.148
Expt.[b]	4.385	3.838	10.825	0.109	0.890	0.481	0.154
Expt.[c]	4.381	3.834	10.847	0.110	0.876	0.504	0.156

[a]Reference 8.
[b]Present work $(\bar{1}06)$ preferred orientation correction.
[c]Present work $(00l)$ preferred orientation correction.

c-axis planes cleave more easily so that the crystallites in the powder are likely to be disk shaped. This will lead to a certain degree of misrepresentation of the relative intensities of the relevant (hkl) reflections.

In the specific case of GeSe in which the layers are normal to the c axis, we expect that the $(00l)$ axis will correspond to the dominant preferred orientation direction. However, it is not guaranteed that this axis will lie exactly along the incident beam direction. We have applied a standard correction[19] to account for the observed preferred orientation effects. We found that out of many trial preferred orientation axes a correction appropriate for pure $(00l)$ preferred orientation fit our data best.

The second best preferred orientation direction was found to be the $(\bar{1}06)$ direction, which we expect to account approximately for misalignment of the $(00l)$ axis. It should be emphasized that the true orientation of the crystallites in the pressure cell is too complex to be described completely by a single preferred orientation axis.

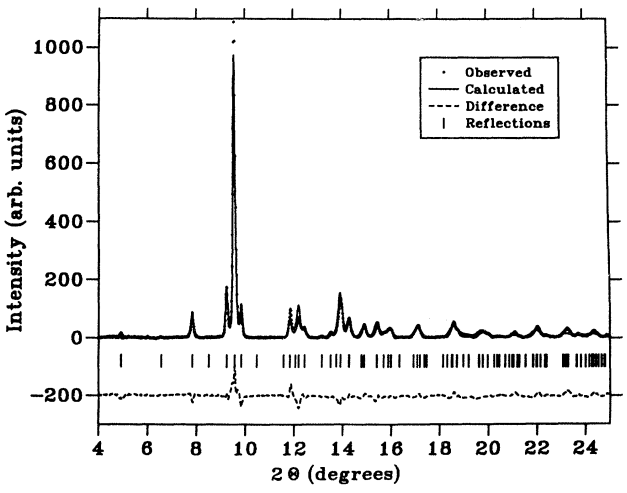

FIG. 4. Rietveld refinement of the powder pattern of GeSe obtained at ambient pressure. The resulting structural parameters are given in Table II. The fit shown here has been obtained using a $(00l)$ preferred orientation correction.

The optimum description should be best done using either several preferred orientation axes or a distribution of such directions. Sophisticated preferred orientation analysis methods are currently being developed to incorporate these distributions.[22,23] It does appear, however, that, in this case, a single preferred direction does provide a reasonable approximation to this distribution. Although it appears that the pure $(00l)$ correction provides the best approximation to the preferred orientation effects in our sample, we have chosen to perform Reitveld refinement of our powder diffraction data, using both pure $(00l)$ and $(\bar{1}06)$ preferred orientation directions for comparison.

Reitveld refinement of the ambient pressure powder pattern using $(00l)$ preferred orientation correction gave the following atomic positional parameters. $u_{Ge} = 0.110$, $v_{Ge} = 0.876$, $u_{Se} = 0.504$, and $v_{Se} = 0.156$. These values are in very good agreement with our calculated results (given above) and with those obtained earlier by single-crystal methods.[8] This agreement also gives us further confidence in the appropriateness of our chosen preferred orientation correction. The ambient pressure results are summarized in Table II in which we also show the structural parameters for GeSe as determined from an earlier single-crystal study. The least-squares fit to the ambient pressure powder profile is shown in Fig. 4

B. Structural response to pressure

We next consider the pressure dependence of the GeSe structure. In Fig. 5 is shown the experimental and calculated fractional compression of the three lattice parameters under hydrostatic pressure. The two sets of experimental data refer to two different sample histories. Specifically, one powder sample was pressurized up to approximately 100 kbar and then decompressed. The open symbols refer to the measured lattice parameters as obtained from this sample upon recompression. The purpose of this initial pressurization was twofold. First, we aimed to establish whether any irreversible pressure-induced phase transition occurred. We found no evidence for any irreversibility as the diffraction profile from the recovered sample was nearly indistinguishable from that of the starting material. Second, initial pressurization might also help to improve the quality of the powder. In

practice, we found that the improvement was not significant. The (+, ×, and *) symbols represent measurements obtained on a fresh GeSe powder sample.

As is evident from the figure, the c axis is not the most compressible of the three. This is somewhat surprising in view of the fact that it is this direction which is normal to the weakly bonded double layers. However, the pressure dependence of our calculated bond angles given in Fig. 6 shows that the angle for the intralayer bond is much softer than the angle for the bond in the a-b plane under pressure. This result suggests that the response to pressure of the GeSe structure proceeds mainly by compression along the a-axis direction — involving bending of the intralayer bonds.

The bulk modulus of GeSe, as determined by our experiments is approximately 431(5) kbar, which is somewhat lower than that reported in Ref. 2. However, it should be noted that the measurements given in Ref. 2 were obtained over a wider pressure range than that performed in the present work.

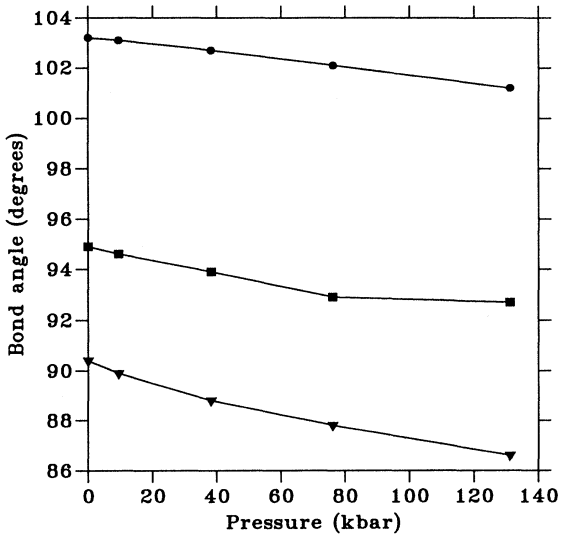

FIG. 6. The calculated hydrostatic pressure response of the bond angles. The response of the bond angle in the a-b plane is shown by solid squares. The response of the other two intralayer bond angles are shown as solid circles and solid triangles. See text for details.

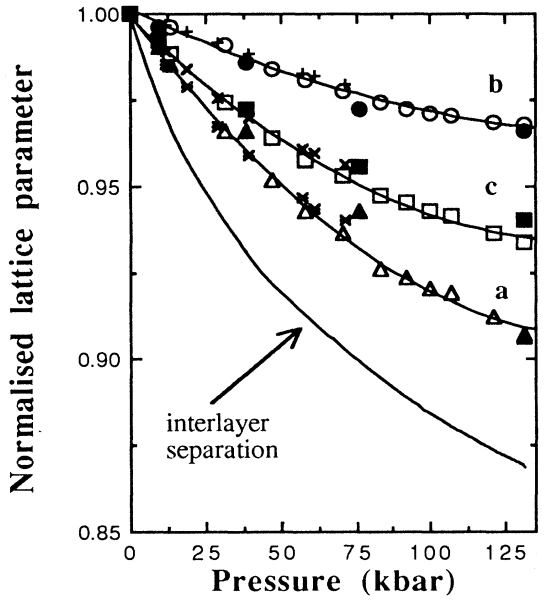

FIG. 5. The dependence of the unit cell parameters a, b, and c as a function of hydrostatic pressure up to 135 kbar. Values have been normalized to those obtained at ambient pressure. Solid symbols represent the calculated values and open symbols (and +, ×, and * symbols) represent experimental points as determined using angle-dispersive powder x-ray diffraction. Experimental data (shown as open symbols) have been collected on pressure increase from a sample initially pressurized to 100 kbar and then decompressed. Experimental data [shown as (+, ×, and *) symbols] have also been obtained on pressure increase, but a fresh sample was used. It can be seen that the b axis corresponds to the least compressible direction, whereas the a axis is most sensitive to pressure. The solid line through the experimental data is a guide to the eye. Also shown in this figure is the calculated normalized interlayer separation $2(1 - v_{Ge})c$ which, as expected, is observed to decrease most rapidly with pressure.

The fractional compression of the interlayer distance however, is found to be most sensitive to pressure as would be expected. This is also shown in Fig 5. The thickness of the double layer is relatively unchanged over this pressure range.

The pressure dependence of the atomic positional parameters has also been studied using both *ab initio* simulations and high-pressure powder diffraction. The results are shown in Figs. 7(a) to (d).

We also show in these figures the differences in the experimentally determined pressure response of the internal parameters, as obtained by using either the pure $(00l)$ or $(\bar{1}06)$ preferred orientation correction. It is clear that the u_{Ge} positional parameter [shown in 7(a)] is largely independent of the choice of preferred axis over the entire pressure range and the ambient pressure value is very close to that determined by single-crystal methods.[8] This is particularly significant as it is this positional parameter that appears to be in best agreement with the results of our theoretical calculations. The trend in the pressure response of the v_{Ge} positional parameter [shown in 7(b)] also appears to be fairly insensitive to the choice of preferred orientation direction. However, the $(\bar{1}06)$ correction leads to an ambient pressure value of the v_{Ge} parameter, which is considerably higher than both the theoretical value and that reported in Ref. 8. The positional parameters for the Se atoms are generally found to be more sensitive to the choice of preferred orientation than are those of the Ge atoms. This is particularly evident for the u_{Se} parameter shown in 7(c). In this figure, it is evident that a correction for preferred orientation in the $(\bar{1}06)$ direction leads to an underestimate of

the u_{Se} parameter over all pressures considered, although the slope du_{Se}/dP is similar for both choices. In this case, we find that the pure (00l) correction leads to results in very good agreement with those of our calculations both in absolute value and slope at all pressures. The ambient pressure value as obtained using this correction is also in very good agreement with the single-crystal data reported in Ref. 8. Both choices of the preferred orientation axis lead to an overestimate of the v_{Se} positional parameter relative to that obtained in our calculations. This is shown in 7(d). Our *calculated* result for the ambient pressure value of this parameter, however, is in

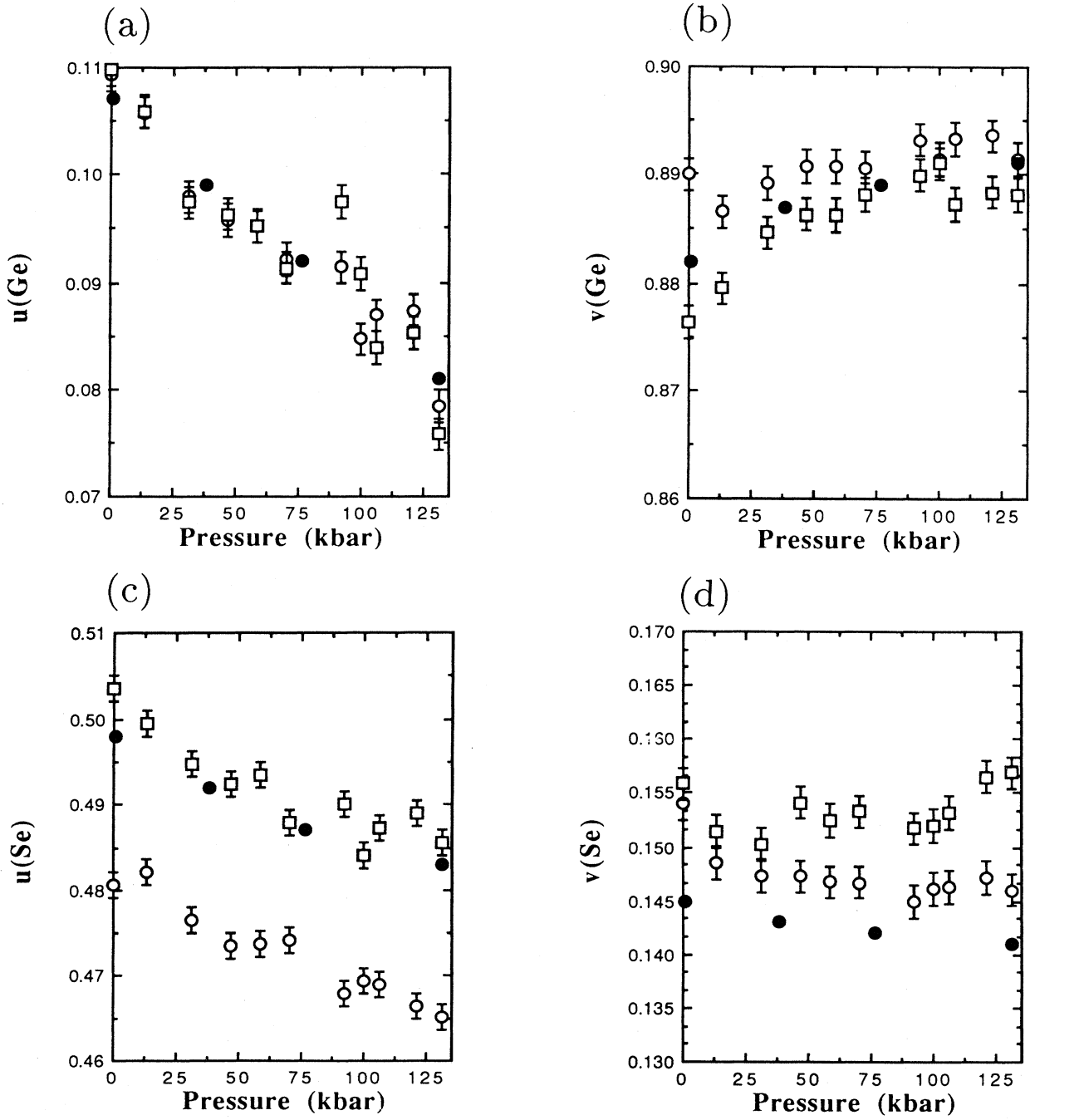

FIG. 7. The variation of the structural parameters u_{Ge}, v_{Ge}, u_{Se}, and v_{Se} with pressure are shown independently in (a), (b), (c), and (d), respectively. Error bars represent the estimated standard deviation. Solid symbols represent the calculated values and open symbols represent experimental points as determined using angle-dispersive powder x-ray diffraction. The open squares have been obtained using a correction appropriate for preferred orientation in the (00l) direction, while open circles have been obtained using ($\bar{1}$06) as the preferred orientation axis.

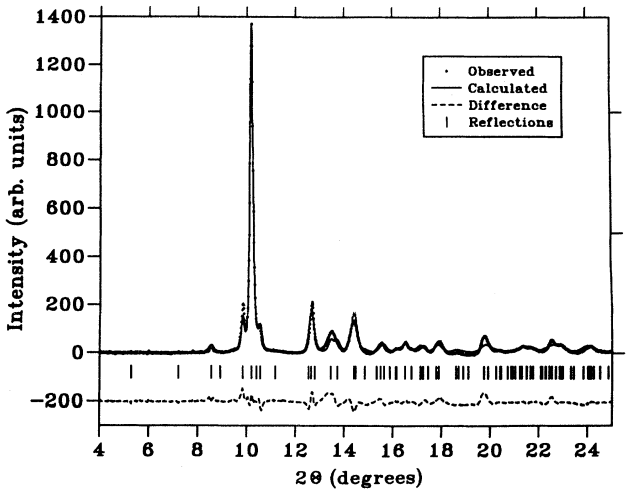

FIG. 8. Rietveld powder profile refinement of the GeSe profile obtained at 130.9 kbar. A correction for preferred orientation along (00l) has been applied.

close accord with that of single single-crystal data.[8] For this parameter, we find that the pressure *trend* obtained using the ($\bar{1}06$) correction is well reproduced in our calculations and that there is considerably more scatter in the results obtained using the pure (00l) correction.

In summary, we find that our density functional total-energy calculations (incorporating unit cell optimization and atom position relaxation) are capable of providing a very detailed, predictive description of pressure response in this complex layered solid. Moreover, an understanding of the origin of the discrepancies (between experiment and theory) in the absolute values of the positional parameters appears to require fairly sophisticated modeling of the distribution of crystallite orientations in the powdered sample. This is presently outside the realm of standard powder diffraction analysis methods.

We now consider the issue of pressure-induced structural phase transitions in GeSe. We find no evidence in these experiments to support the claim that GeSe undergoes a pressure-induced first-order structural phase transition to a metallic modification at approximately 60 kbar, as was reported earlier by Bhatia *et al.* on single-crystal GeSe. We have taken our GeSe samples up to a maximum pressure of 130 kbar. The diffraction pattern recorded at this pressure is shown along with a least-squares fit in Fig. 8. As stated earlier, decompression to ambient pressure resulted in a diffraction pattern almost identical to that obtained from the starting material albeit with slightly broadened peaks. It is possible that if sufficient nonhydrostaticity was present in the experiment described in Ref. 5 this could have initiated a transition that is otherwise absent in a more hydrostatic environment.

We find no experimental evidence in these studies to support the claim made in Ref. 5 that a NaCl-like structure is formed upon decompression. We have also performed total energy calculations on GeSe in the NaCl structure, which further suggest that the equilibrium lat-

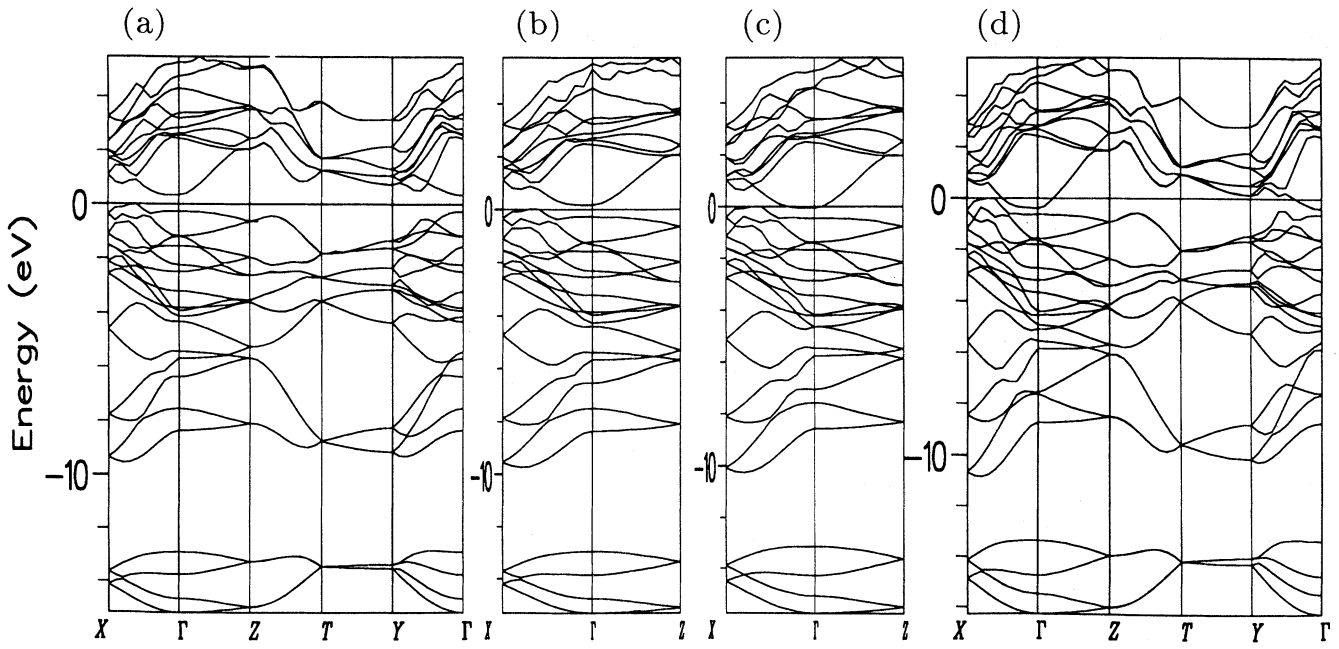

FIG. 9. Evolution of the valence electron band structure of GeSe as determined at 0, 9.5, 38.2, and 76.2 kbar are shown in (a), (b), (c), and (d), respectively. It is evident that a pressure-induced closure of the indirect band gap is predicted in these calculations. This gap closure may be responsible for the observed large drop in electrical resistivity in GeSe reported in Ref. 5.

tice parameter of NaCl-like GeSe would be 5.483 Å, which is substantially smaller than the value reported in Ref. 5.

We, therefore, believe that the phase transitions reported in Ref. 5 are the result of nonhydrostaticity and that the recovered sample has a structure that is more complex than NaCl. In the next section, we consider the variation of the electronic band structure of GeSe under hydrostatic pressure.

VI. ELECTRONIC STRUCTURE

A. Band structure

We have calculated the electronic energy band structure of GeSe at several pressures and the response of the electronic structure to pressure is shown in Fig. 9. In both cases the band structures were calculated from fully relaxed atom positions and unit cell parameters. Unlike variational total-energy calculations, the evaluation of the band structure requires matrix diagonalization. This diagonalization is performed at many k points along high-symmetry directions in the Brillouin zone (see Fig. 10), but the Hamiltonian is based on the original, self-consistent charge density as determined by the 20 k-point calculation. At ambient pressure, we find that GeSe has an indirect band gap of 0.35 eV, as compared to the experimental value of 1.53 eV. This underestimate is to be expected in view of the well-known inadequacies of density functional theory in correctly accounting for the excited electronic states of solids. As is evident from these figures, the electronic energy gap decreases with increasing pressure. At a pressure of approximately 40 kbar, the conduction band at the Γ point overlaps the top of the valence band along the Σ line of the Brillouin zone. This, therefore, corresponds to a pressure-induced semiconductor-to-semimetal phase transition. This may explain the observed large drop in electrical resistivity at 60 kbar reported by Ref. 5 We should emphasize that, in view of the well-known inadequacies of density functional theory in predicting excited state energy levels, we feel that our calculated metallization pressure is subject to large a error.

B. Valence charge densities

We have also investigated the valence electron charge distribution in GeSe, with a view to understanding the nature of the bonding in this anisotropic material. The three-dimensional valence charge density is shown in Figs. 11(a) and (b). Four unit cells (doubled along the a and b axes) are shown. It can be seen in this figure that the atoms in a single double layer are covalently bonded in threefold coordination. It is also clear from the figure that there is considerable electron density centered around the individual atom positions in addition to being shared in the bonds. In Fig. 11(a), it can be seen that there is negligible electron density between the layers. These charge density plots were obtained from the ambient pressure structure. At compressed volumes, slight bridging of the electron distribution across the in-

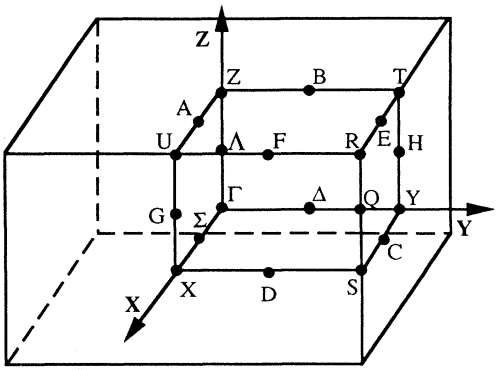

FIG. 10. Brillouin zone for the primitive orthorhombic structure showing the labeling conventions for high-symmetry points and directions. In this convention, the x, y, and z directions correspond to a, b, and c crystallographic axes, respectively.

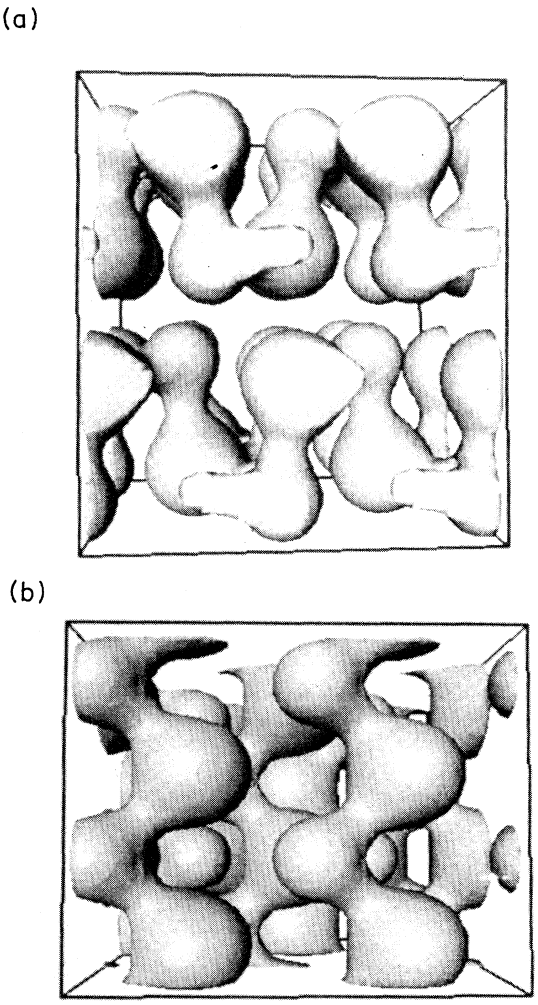

FIG. 11. Valence charge distribution in GeSe as viewed perpendicular to the c axis (a) and parallel to the c axis (b). As can be seen in the figure, each atom is threefold coordinated via covalent bonds within a given double layer. It is evident from (a) that there is negligible covalent bonding between layers.

terlayer gap is observed. It should be noted that the van der Waals interaction is not included in our calculations and yet the cohesion appears to be quite well described.

VII. VIBRATIONAL PROPERTIES

We have investigated the vibrational frequency of the A_g shear mode as a function of pressure within the rigid-layer-mode approximation. We begin the calculation by obtaining the fully relaxed GeSe structure at the equilibrium volume. A small displacement of one of the GeSe layers is made and the restoring force corresponding to that displacement is then calculated. This procedure is then repeated at several points along the hydrostatic curve. In these calculations, it is particularly important to converge the Hellmann-Feynman forces sufficiently such that only a small displacement has a measurable effect.

The calculated shear mode vibrational frequency at ambient pressure is found to be 47 cm^{-1}, respectively. The experimental Raman scattering results of Ref. 10 give the frequency of the A_g shear mode as 40 cm^{-1} at room temperature and at 43 cm^{-1} at 20 K. Our *ab initio* calculations are, therefore, in good agreement with these experimental results and it is clear that temperature effects are small but non-negligible. We next investigate the pressure dependence of these frequencies.

The calculated shear mode frequency as a function of hydrostatic pressure is shown in Fig. 12. We also show the results of our high-pressure Raman scattering measurements of the A_g shear mode. It is clear from these plots that although the calculated ambient pressure shear mode frequency is in reasonable accord with the experimental results, the frequency of this vibration at high pressure is severely overestimated in our calculations. For example, by 40 kbar, the calculated shear mode frequency is overestimated by more than 30% in the calculation, whereas the overestimate was only about 20% for the ambient pressure frequency. The origin of this discrepancy is not immediately clear, but several causes are possible. For example, it may be that the underestimate of the unit cell volume has the effect of stiffening the bonds. However, the agreement between the calculated and experimental pressure response of the internal structure suggests that this effect is not large. It may also be that the rigid-layer-mode approximation is not valid in the case of GeSe and that non-negligible coupling between interlayer and intralayer vibrations exists. The frequency of the A_g shear mode is shown as a function of pressure in Fig. 12.

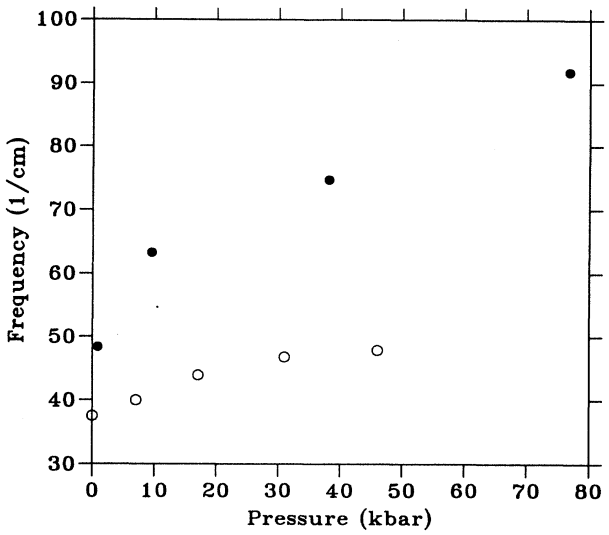

FIG. 12. The observed (open circles) and calculated (solid circles) hydrostatic pressure variation of the A_g shear phonon frequency, as calculated using the rigid-layer approximation.

VIII. CONCLUSION

We have reported an extensive theoretical and experimental study of high-pressure effects in the layered IV-VI semiconductor GeSe, using a combination of angle-dispersive powder x-ray diffraction, Raman scattering and first-principles density functional pseudopotential calculations. Our general observations are that density functional techniques are capable of adequately describing not only the equilibrium structural and vibrational properties in this highly anisotropic solid, but are also very effective in predicting detailed pressure-induced changes in the unit cell and atomic positions. More specifically, we find neither computational nor experimental evidence to support earlier claims of a strongly first-order structural transition to a metallic phase at 60 kbar although our electronic structure calculations are consistent with a pressure-induced closure of the band gap at elevated pressure.

ACKNOWLEDGMENTS

The authors are grateful to R.J. Nelmes, M.I. McMahon, and D.R. Allan for invaluable assistance with the high-pressure x-ray experiments and to E. Schönherr for providing us with a sample of GeSe. J.C. and G.J.A. acknowledge support from the Royal Society of Edinburgh. J.C. also thanks the EPSRC and the Royal Society of London. S.J.C. thanks the EPSRC for support. H.C.H. thanks the Overseas Research Studentship scheme for support and M.C. Warren and J.R. Maclean for helpful discussions.

[1]P.B. Littlewood, J. Phys. C **13**, 4855 (1980).

[2]T. Chattopadhyay, A. Werner, and H.G. von Schnering, in *High Pressure in Science and Technology,* edited by C. Homan, R.K. MacCrone, and E. Whalley, MRS Symposia Proceedings No. 22 (Materials Research Society, Pittsburgh, 1984), p. 93.

[3]Recent high-resolution powder diffraction studies have revealed that the high-pressure structures of the Pb chalco-

genides exhibit slight monoclinic distortions from the GeS-type structure. J.R. Maclean, P.D. Hatton, R.O. Piltz, J. Crain, and R.J. Cernik, Nucl. Instrum. Methods B (to be published).
[4]Y. Fujii, K. Kitamura, A. Onodera, and Y. Yamada, Solid State Commun. **49**, 135 (1984).
[5]K.L. Bhatia, G. Parthasarathy, D.P. Gosain, and E.S.R. Gopal, Phys. Rev. B **33**, 1492 (1986).
[6]R. Zallen and M. Slade, Phys. Rev. B **9**, 1627 (1974).
[7]H.R. Chandrasekhar, R.G. Humphries, and M. Cardona, Phys. Rev. B **16**, 2891 (1977).
[8]A. Okazaki, J. Phys. Soc. Jpn. **13**, 1151 (1958).
[9]H.R. Chandrasekhar and U. Zwick, Solid State Commun. **18**, 1509 (1976).
[10]T. Fukunaga, S. Sugai, T. Kinosada, and K. Murase, Solid State Commun. **38**, 1049 (1981).
[11]S.V. Vlachos, A.P. Lambros, A. Thanailkis, and N.A. Economou, Phys. Status Solidi **76**, 727 (1976).
[12]M.P. Lisistra, A.P. Zakharchuk, S.F. Terekhova, G.G. Tsebulya, L.K. Mladov, and S.M. Todorov, Phys. Status Solidi **75**, K51 (1976).
[13]S. Asanabe and A. Okazaki, J. Phys. Soc. Jpn. **13**, 1151 (1958).
[14]J.P. Perdew and A. Zunger, Phys. Rev. B **23**, 5048 (1981).
[15]L. Kleinman and D.M. Bylander, Phys. Rev. Lett. **20**, 1425 (1982).
[16]G.P. Kerker, J. Phys. C **13**, L189 (1980).
[17]H.J. Monkhorst and J.D. Pack, Phys. Rev. B **13**, 5188 (1976).
[18]M.C. Payne, M.P. Teter, D.C. Allan, T.A. Arias, and J.D. Joannopolous, Rev. Mod. Phys. **64**, 1045 (1992).
[19]A. Fitch and A.D. Murray (unpublished).
[20]R.J. Nelmes and M.I. McMahon, J. Synchrotron Rad. **1**, 69, 1994.
[21]R.O. Piltz, M.I. McMahon, J. Crain, P.D. Hatton, R.J. Nelmes, R.J. Cernik, and G. Bushnell-Wye, Rev. Sci. Instrum. **63**, 700 (1992).
[22]N.G. Wright, Ph.D. thesis, The University of Edinburgh, 1994.
[23]Y. Ishihara, Y. Ohno, and I. Nakada, Phys. Status Solidi B **121**, 407 (1984).

(a)

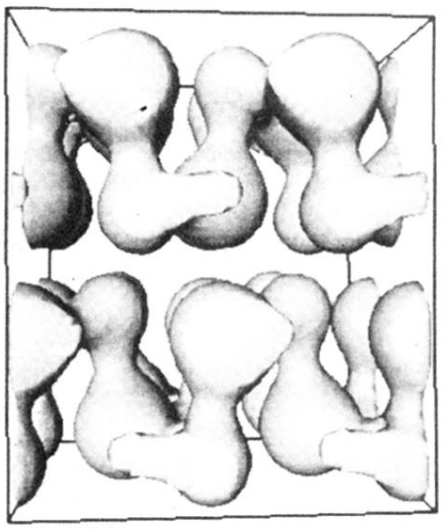

(b)

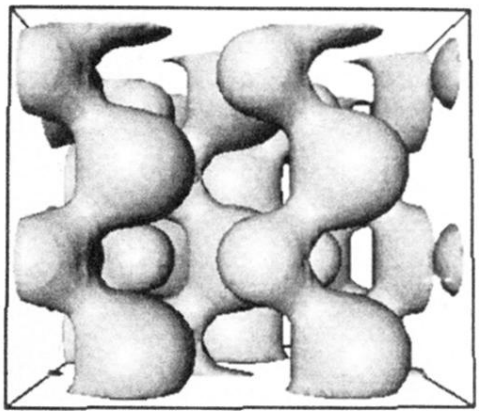

FIG. 11. Valence charge distribution in GeSe as viewed perpendicular to the c axis (a) and parallel to the c axis (b). As can be seen in the figure, each atom is threefold coordinated via covalent bonds within a given double layer. It is evident from (a) that there is negligible covalent bonding between layers.